IEICE TRANS. COMMUN., VOL.E100–B, NO.10 OCTOBER 2017

INVITED PAPER *Joint Special Section on Opto-electronics and Communications for Future Optical Network*

MFD Measurement of a Six-Mode Fiber with Low-Coherence Digital Holography

Yuta WAKAYAMA[†a)], ***Member***, **Hidenori TAGA**[†], ***and*** **Takehiro TSURITANI**[†], ***Senior Members***

SUMMARY This paper presents an application of low-coherence interferometry for measurement of mode field diameters (MFDs) of a few-mode fiber and shows its performance compared with another method using a mode multiplexer. We found that the presented method could measure MFDs in a few-mode fiber even without any special mode multiplexers.

key words: *few-mode fiber, mode field diameter, low-coherence digital holography, mode-division multiplexing*

1. Introduction

Few-mode fibers (FMFs) are developed aiming at increasing transmission capacity synergistically with mode-division multiplexed (MDM) transmission techniques [1]–[3]. Such MDM transmission systems using FMFs are considerably affected by modal crosstalk (MXT) and mode-dependent loss (MDL) [4]–[8]. The MXT and MDL are induced by mismatching of mode fields at splicing/contacting points of few-mode fibers/devices; therefore, the estimation of mode field mismatching is necessary to design and develop few-mode components and MDM systems. Mismatching of mode fields can be evaluated by mode-field diameters (MFDs) or effective areas (A_{eff}) [9]–[11]; however, conventional measurement methods were determined for single-mode fibers (SMFs) and cannot be applied directly for FMFs since these parameters should be individually considered for each guided mode. In general, the MFDs/A_{eff} of existing modes in an FMF can be measured by separately exciting each mode in the FMF; however, these parameters cannot be measured correctly in the case when MXT at a mode exciter/multiplexer is considerably large [12]. This means that MFD measurements need various mode multiplexers, which are optimized for difference of FMF designs.

In this paper, we focus on MFD measurement and show that low-coherence digital holography (LCDH) [13], [14] can be used as a technique for estimation of MFDs. By using LCDH, a mode exciter with an extremely low MXT is no longer required because randomly excited modes can be recognized in the time domain and near-field patterns (NFPs) of each mode can be captured at the same time. Firstly, we described an MFD definition in FMFs. Secondly, we measured MFDs of a six-mode fiber from NFPs for each mode using a mode multiplexer. Thirdly, we measured the MFDs of the same fiber with LCDH. Finally, the performances of the two methods were compared and discussed.

Manuscript received December 12, 2016.
Manuscript revised March 16, 2017.
Manuscript publicized April 20, 2017.

[†]The authors are with KDDI Research, Inc., Fujimino-shi, 356-8502 Japan.
a) E-mail: yu-wakayama@kddi-research.jp

DOI: 10.1587/transcom.2017OBI0004

2. Moe-Field Diameter in Few-Mode Fibers

In standard SMFs, the MFD is determined by

$$d_{\mathrm{n}} = 2\sqrt{\frac{2\int I(r)r^3dr}{\int I(r)rdr}} \tag{1}$$

where $I(r)$ is a near field optical intensity in the radial direction $r \geq 0$. Equation (1) is widely used [9]–[11]; however, it is applied only for circularly symmetric mode fields.

For noncircularly symmetric fibers or higher-order modes, MFDs can be evaluated as second-order moments [15]

$$w_{\mathrm{x}}^2 = 4\frac{\iint I(x,y)(x-x_0)^2dxdy}{\iint I(x,y)dxdy} \tag{2}$$

and

$$w_{\mathrm{y}}^2 = 4\frac{\iint I(x,y)(y-y_0)^2dxdy}{\iint I(x,y)dxdy}, \tag{3}$$

where $I(x, y)$ is an image of the NFP emitted from a fiber under test, x and y are the horizontal direction and the vertical direction on the captured images, respectively, and x_0 and y_0 are the center positions of the electric distribution on x and y coordinates, respectively. The center positions are calculated as first-order moments

$$x_0 = \frac{\iint I(x,y)xdxdy}{\iint I(x,y)dxdy} \tag{4}$$

and

$$y_0 = \frac{\iint I(x,y)ydxdy}{\iint I(x,y)dxdy}, \tag{5}$$

respectively. By coordinating the center position of a mode field with the center of the NFP, Eqs. (4) and (5) are negligible, i.e., $(x_0, y_0) = (0, 0)$. From Eqs. (2) and (3) the MFDs can be estimated in the x and y directions. Nevertheless, guided modes in FMFs inherently fluctuate by inter-modal interference. In particular, an NFP of a degenerate mode is unstable by the interference between degenerate modes. To

avoid such uncertainty for the MFD measurement of degenerate modes, the effective mode radius [16]

$$w_{\text{off}}^2 = \frac{w_x^2 + w_y^2}{2} \tag{6}$$

can be used, which is stable regardless of degenerate modes. By substituting Eqs. (2) and (3) into Eq. (6), effective mode diameter $d_{\text{eff}} = 2w_{\text{eff}}$ can be written as

$$d_{\text{eff}} = 2\sqrt{\frac{2\iint I(x,y)[(x-x_0)^2 + (y-y_0)^2]dxdy}{\iint I(x,y)dxdy}}. \tag{7}$$

This definition holds the $1/e^2$ intensity diameter for a Gaussian distribution (fundamental mode LP_{01}) as with Eq. (1).

3. Experimental Setups for MFD Measurement

3.1 Setup with a Mode Multiplexer

Figure 1 shows an experimental setup for measurement of MFDs in a six-mode fiber with a mode multiplexer. The mode multiplexer used in this evaluation is based on a multi-plane light conversion [17] and its MXT is lower than −15 dB. The measured fiber was designed with a graded-index profile with a relative index difference of 1.1%, a core diameter of 17.6 μm, and alpha parameter of 1.93 so as to propagate four LP modes (six spatial modes). The designed values of the MFDs for LP_{01}, LP_{11}, LP_{21}, and LP_{02} at the wavelength of 1550 nm were 8.9 μm, 12.8 μm, 16.2 μm, and 16.5 μm, respectively. As a probe light, a broadband amplified spontaneous emission source was filtered into a Gaussian-shape spectrum at the center wavelength of 1550 nm with the full width at a half maximum (FWHM) bandwidth of 10 nm. The probe light was sequentially connected to the input ports of the mode multiplexer as exciting four LP modes individually. After the sample fiber, the probe light was collimated by an objective lens and its NFP was captured by the near infrared camera constructed with the detector array of InGaAs. This camera has a dynamic range of 14 bits, i.e., the pixel values were ranged from 0 to $2^{14} - 1$. The pixel size and the number of pixels were 30×30 μm^2 and 320×256, respectively. The MFDs were evaluated from the NFP of each mode with the determination of Eq. (7). In general, image $I(x, y)$ includes the background noise of the camera caused by dark current, bias noise, background light, and so forth. In the evaluation of Eq. (7), image data of the background noise was captured by shutting out the probe light, and it was subtracted from $I(x, y)$ for maximizing the peak signal-to-noise ratio (PSNR). A variable optical attenuator (VOA) was used for changing power of the probe light when evaluating the MFDs for different PSNRs.

3.2 Setup with Low-Coherence Digital Holography

In the MFD measurement with low-coherence digital holography, the probe light was generated in the same way with

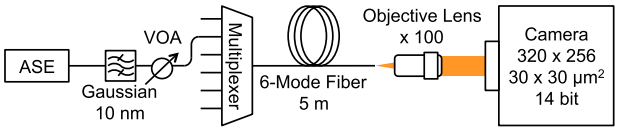

Fig. 1 Experimental setup for MFD measurement with a mode multiplexer.

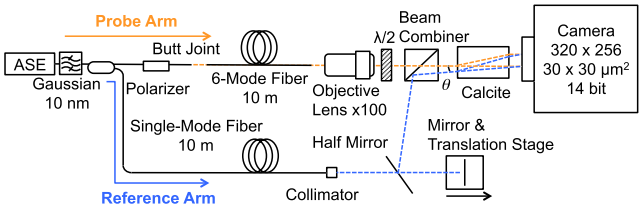

Fig. 2 Experimental setup for MFD measurement with low-coherence digital holography.

the setup using a mode multiplexer, as shown in Fig. 2. The filtered light was divided into a probe arm and a reference arm. The probe light and the reference light were entered into the six-mode fiber and a standard single-mode fiber, respectively. On the probe arm, the emitted light from the fiber under test was collimated with the objective lens and separated into two polarizations by a calcite. On the reference arm, the length of the light path was shifted by a translation stage for scanning the temporal delay of each mode in the fiber under test. The step size of the translation stage and the bandwidth of the light source determine the resolution in the time region. Consequently, the NFP can be evaluated by

$$I(x, y; \tau) = |f(x, y; \tau)|^2 = |\text{IFFT}[F(x, y; \tau)]|^2 \tag{8}$$

where

$$F(x, y; \tau) = \text{FFT}\left[\frac{h(x, y; \tau)}{\sqrt{I_r(x, y)}\exp(-i\theta)}\right] W \tag{9}$$

and

$$h(x, y; \tau) = I_f(x, y; \tau) - [I_p(x, y) + I_r(x, y)]. \tag{10}$$

Here, τ is temporal delay corresponding to the relative position of the translation stage, θ is the angle between the probe light and the reference light on the camera, W is a circular window function for extraction of a mode field $f(x, y; \tau)$, $h(x, y; \tau)$ is a holographic pattern, $I_f(x, y; \tau)$ is an interference fringe, $I_p(x, y)$ and $I_r(x, y)$ are the intensity distribution of the probe light and the reference light, respectively. By subtracting $I_p(x, y) + I_r(x, y)$ from $I_f(x, y; \tau)$ in advance, the DC component can be reduced and effectively filtered out with the window function W. In this experiment, the angle θ was set ~0.7°.

4. Results and Discussion

4.1 MFD Measurement with a Mode Multiplexer

Firstly, we evaluated the MFDs with a mode multiplexer.

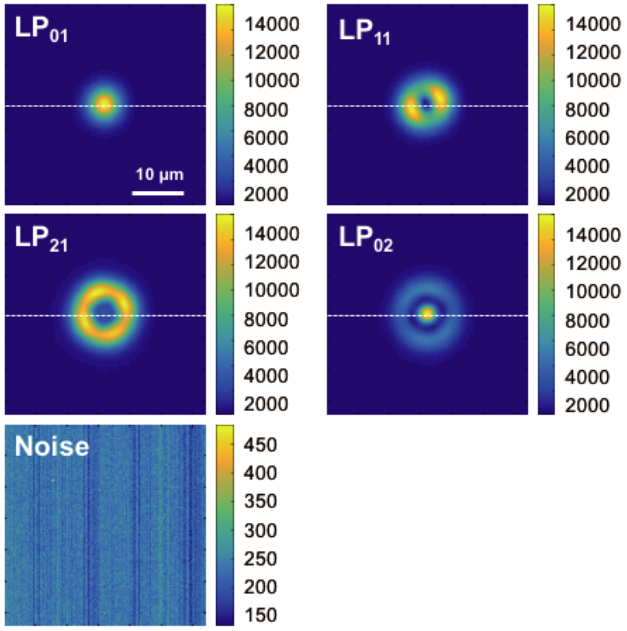

Fig. 3 Near-field patterns with a mode multiplexer and noise image when blocking out the probe light.

Figure 3 shows NFPs and a background image, which were averaged over ten measurements with the setup in Fig. 1. The intensity distribution of each mode was mingled with their degenerate modes and shaped as a spot and/or a ring by using a low-coherence light source. Figure 4 presents the intensity distribution on the horizontal axis of Fig. 3 (dashed line) for four LP modes. The average value of the background noise was ∼200. This noise level deteriorates PSNR and causes measurement error because Eq. (7) includes integrals over whole images [16]. Indeed, without subtraction of the noise image, the MFDs of LP_{01}, LP_{11}, LP_{21}, and LP_{02} were estimated from Eq. (7) as 30.8 μm, 26.0 μm, 23.6 μm, and 30.2 μm, respectively. These MFD values were obviously overestimated compared to those in Fig. 4. In contrast, with subtraction of the noise image, the average noise level could be reduced from ∼200 to ∼3; thus, the MFDs were calculated as 10.5 μm, 12.7 μm, 15.5 μm, and 16.3 μm, respectively.

4.2 MFD Measurement with Low-Coherence Digital Holography

Next, we demonstrate the performance of the LCDH for MFD measurement. Figure 5 shows an impulse response calculated by the integral of $|f(x, y; \tau)|^2$ as a function of τ. In the time domain, the FWHM of LP_{01} was 0.5 ps; thus, every mode of the six-mode fiber could be recognized even without a mode multiplexer. The NFPs of LP_{01}, LP_{11}, LP_{21}, and LP_{02} were observed at τ = 0 ps, −1.3 ps, −16.8 ps, and −28.8 ps, respectively, indicated with arrows. Figure 6 shows examples of captured images. The fringe image $I_f(x, y; \tau)$ was observed at the relative time τ of −28.8 ps in the impulse response. The reference image $I_r(x, y)$ was captured while blocking out the probe light. The image without fringe patterns $I_p(x, y) + I_r(x, y)$ was captured when the translation stage was significantly shifted from each peak in the impulse response. Holographic pattern $h(x, y; \tau)$ was obtained by Eq. (10). From these images, the complex amplitude $f(x, y; \tau)$ of LP_{02} was clearly extracted using Eqs. (8)–(10), as shown in Fig. 7. By FFT for $h(x, y; \tau)$, a residual DC component, a desired mode field, and a conjugation of the mode field were separated on different angles [Fig. 7(a)]. The desired mode field was shifted onto the center in the Fourier plane by adjusting θ in Eq. (9) and extracted by the window function W [Fig. 7(b)]. In this process, NFPs depend on the size of the aperture on the Fourier plane. To decide the aper-

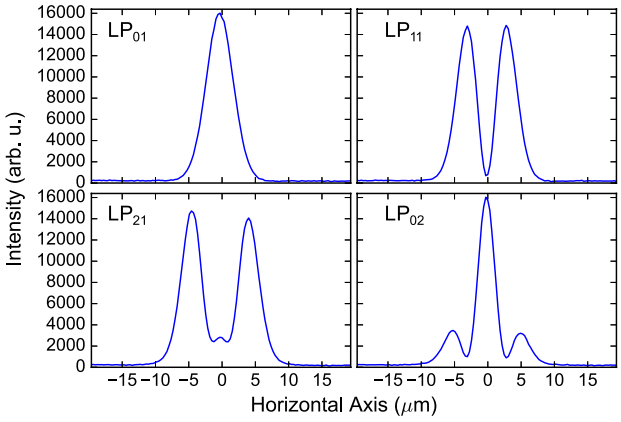

Fig. 4 Intensity distribution on horizontal axis.

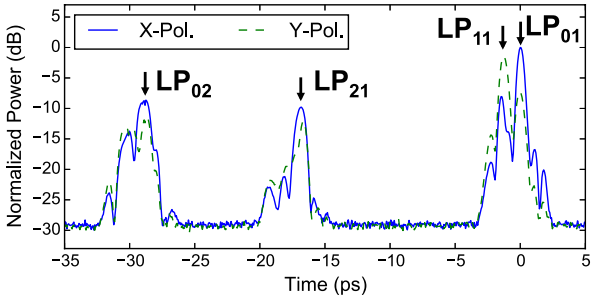

Fig. 5 An impulse response of the six-mode fiber.

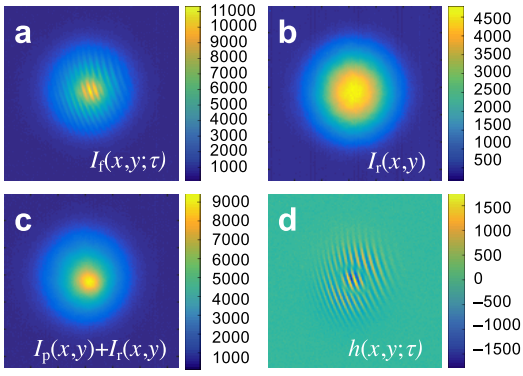

Fig. 6 Examples of images. (a) interference pattern $I(x, y; \tau)$, (b) reference intensity $I_r(x, y; \tau)$, (c) DC component $I_p(x, y) + I_r(x, y)$, and (d) holographic pattern $h(x, y; \tau) = I(x, y; \tau) - I_p(x, y) - I_r(x, y)$.

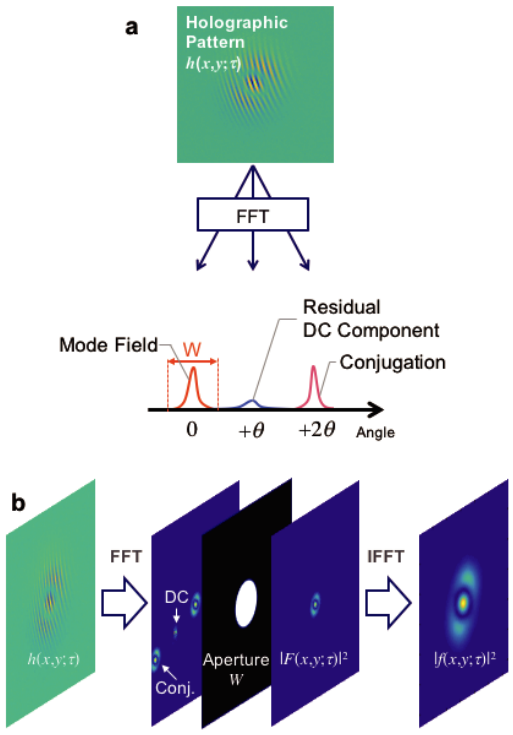

Fig. 7 Examples of Fourier analysis. (a) FFT of holographic pattern $h(x, y; \tau)$ and (b) Extracting a mode field from a hologram.

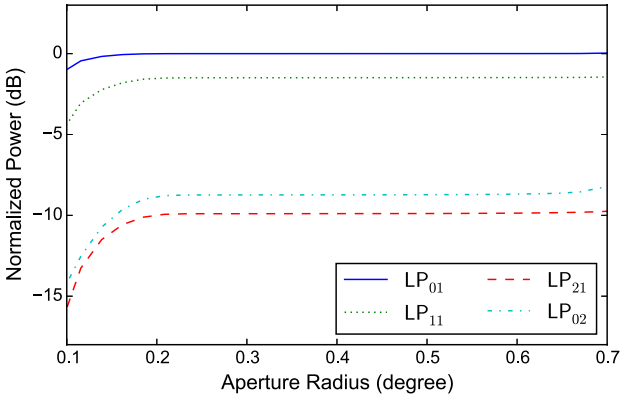

Fig. 8 Normalized power after different aperture radii.

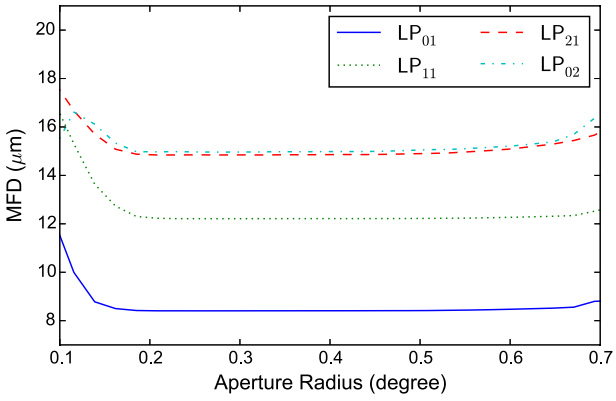

Fig. 9 Mode Field Diameters (MFDs) for different aperture radii.

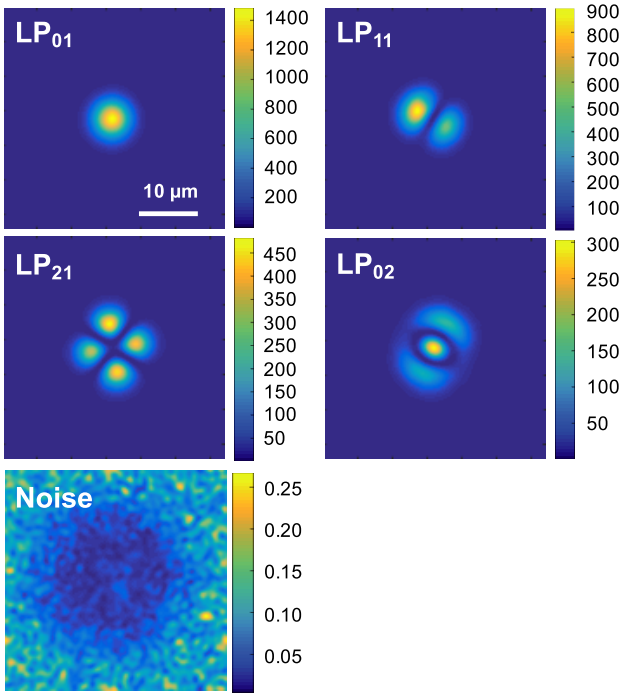

Fig. 10 Near-field patterns for evaluation of MFD with low-coherence digital holography.

ture size, power after the window function was calculated for different aperture radii, as shown in Fig. 8. MFDs were also calculated by changing the aperture size, as shown in Fig. 9. According to these results, power and MFDs were almost constant over the aperture radius of 0.2° and these values were slightly increased around the aperture radius of 0.7° because of the incoming residual DC component. Figure 10 shows mode field images obtained from Eq. (8) with the aperture radius of 0.36°. The NFPs of LP modes were obtained at the relative time indicated with arrows in Fig. 5. A noise image was computationally obtained from an image of $I_p(x, y) + I_r(x, y)$ using the same parameter set with the images of LP modes. As with the previous section, accuracy of MFD evaluation can be improved by subtracting the noise image from the NFPs. Compared to those shown in Fig. 3, the noise level was dramatically suppressed thanks to the window function and intensity compensation by the probe and reference images. As a result, the MFDs of LP_{01}, LP_{11}, LP_{21}, and LP_{02} were obtained as 8.5 μm, 12.2 μm, 14.8 μm, and 15.0 μm, respectively.

4.3 Comparison of MFD Measurements with a Mode Multiplexer and Low-Coherence Digital Holography

Finally, the aforementioned MFD measurements were compared based on PSNR as shown in Fig. 11. The open symbols show the measured MFDs with the mode multiplexer while adjusting the incident power of the probe light by VOA shown in Fig. 1. The MFDs measured with LCDH are plotted as

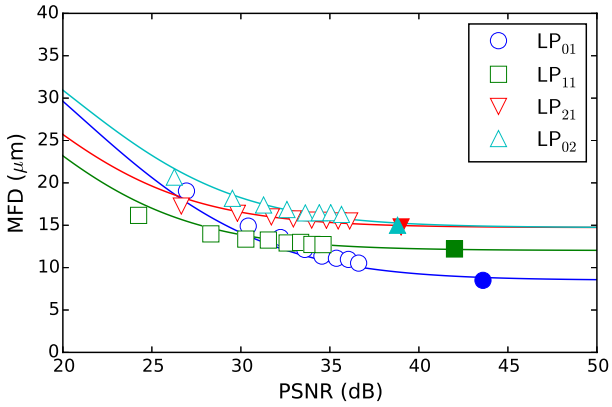

Fig. 11 Measured MFD vs. PSNR with a mode multiplexer (open symbols) and low-coherence digital holography (closed symbols).

closed symbols. The four curves were numerically obtained from Hermite-Gaussian functions [18]. These curves were in good agreement with both the open and closed symbols. According to the curves and the symbols, the accuracy of the MFD measurements seriously deteriorated when PSNR was lower than ~35 dB. The maximum of PSNR was limited due to the dynamic range of the camera and the residual noise level after subtraction of the noise image. For the open symbols, the maximum of PSNR did not reach to 40 dB while the signal peak powers were monitored with the camera for maximizing them. In contrast, although LCDH used a large portion of the dynamic range of the camera for the DC component, we found that PSNRs were improved from 38.8 dB to 43.6 dB for the closed symbols because the noise level was successfully reduced to less than 1.0 as shown in Fig. 10. This result indicates that an optimized mode multiplexer is no longer required for the measurement of MFDs in an FMF by using LCDH.

5. Conclusions

We measured the MFDs of six-mode fibers with the proposed low-coherence interferometer and presented a performance comparison between the proposed method and a general method using a mode multiplexer. We found that the MFDs of the FMF could be measured by LCDH even without a mode multiplexer.

Acknowledgments

Some of the research results have been achieved by the Commissioned Research of the National Institution of Communications Technology (NICT), Japan.

References

[1] L. Grüner-Nielsen, Y. Sun, J.W. Nicholson, D. Jakobsen, K.G. Jespersen, R. Lingle, Jr., and B. Pálsdóttir, "Few mode transmission fiber with low DGD, low mode coupling, and low loss," J. Lightwave Technol., vol.30, no.23, pp.3693–3698, 2012.

[2] T. Hayashi, T. Nagashima, K. Yonezawa, Y. Wakayama, D. Soma, K. Igarashi, T. Tsuritani, T. Taru, and T. Sasaki, "Six-mode 19-core fiber with 114 spatial modes for weakly-coupled mode-division-multiplexed transmission," J. Lightwave Technol., vol.35, no.4, pp.748–754, 2016.

[3] T. Sakamoto, T. Matsui, K. Saitoh, S. Saitoh, K. Takenaga, T. Mizuno, Y. Abe, K. Shibahara, Y. Tobita, S. Matsuo, K. Aikawa, S. Aozasa, K. Nakajima, and Y. Miyamoto, "Low-loss and low-DMD few-mode multi-core fiber with highest core multiplicity factor," The Optical Fiber Communication Conference and Exhibition, Th5A.2, 2016.

[4] T. Mizuno, H. Takara, K. Shibahara, A. Sano, and Y. Miyamoto, "Dense space division multiplexed transmission over multicore and multimode fiber for long-haul transport systems," J. Lightwave Technol., vol.34, no.6, pp.1484–1493, 2016.

[5] R. Ryf, S. Randel, A.H. Gnauck, C. Bolle, A. Sierra, S. Mumtaz, M. Esmaeelpour, E.C. Burrows, R.-J. Essiambre, P.J. Winzer, D.W. Peckham, A.H. McCurdy, and R. Lingle, "Mode-division multiplexing over 96 km of few-mode fiber using coherent 6×6 MIMO processing," J. Lightwave Technol., vol.30, no.4, pp.521–531, 2012.

[6] D. Soma, Y. Wakayama, S. Beppu, K. Igarashi, T. Tsuritani, H. Taga, I. Morita, and M. Suzuki, "665 and 947 b/s/Hz ultra-highly aggregate-spectral-efficient SDM/WDM transmission over 6-mode 19-core fibre using DP-16QAM/64QAM signals," 42nd European Conference and Exhibition on Optical Communications (ECOC), Th.3.C.2, 2016.

[7] J. Vuong, P. Ramantanis, Y. Frignac, M. Salsi, P. Genevaux, D.F. Bendimerad, and G. Charlet, "Mode coupling at connectors in mode-division multiplexed transmission over few-mode fiber," Opt. Express, vol.23, no.2, pp.1438–1455, 2015.

[8] D.M. Marom, J. Dunayevsky, D. Sinefeld, M. Blau, R. Ryf, N.K. Fontaine, M. Montoliu, S. Randel, C. Liu, B. Ercan, M. Esmaeelpour, S. Chandrasekhar, A.H. Gnauck, S.G. Leon-Saval, J. Bland-Hawthorn, J.R. Salazar-Gil, Y. Sun, L. Grüner-Nielsen, and R. Lingle, "Wavelength-selective switch with direct few mode fiber integration," Opt. Express, vol.23, no.5, pp.5723–5737, 2015.

[9] K. Petermann and R. Kühne, "Upper and lower limits for the microbending loss in arbitrary single-mode fibers," J. Lightwave Technol., vol.4, no.1, pp.2–7, 1986.

[10] ITU-T G.650.2, "Definitions and test methods for statistical and nonlinear related attributes of single-mode fibre and cable." Aug. 2015.

[11] M. Artiglia, G. Coppa, P. Di Vita, M. Potenza, and A. Sharma, "Mode field diameter measurement in single-mode optical fibers," J. Lightwave Technol., vol.7, no.8, pp.1139–1152, 1989.

[12] T. Hayashi, Y. Tamura, T. Nagashima, K. Yonezawa, T. Taru, K. Igarashi, D. Soma, Y. Wakayama, and T. Tsuritani, "Effective area measurement of few-mode fiber using far field scan technique with Hankel transform generalized for circularly-asymmetric mode," Frontiers in Optics (FiO), FTh5E.3, 2016.

[13] Y. Wakayama, H. Taga, K. Igarashi, and T. Tsuritani, "DMD measurement of 114-SDM transmission fibre using low-coherence interferometry with digital holographic processing," 41st European Conference and Exhibition on Optical Communications (ECOC), P.1.19, 2015.

[14] Y. Wakayama, H. Taga, and T. Tsuritani, "MFD measurement of a six-mode fiber with low-coherence digital holography," 21st Optoelectronics and Communications Conference/International Conference on Photonics in Switching 2016 (OECC/PS2016), ThC2-3, 2016.

[15] K. Hayata, M. Koshiba, and M. Suzuki, "Modal spot size of axially nonsymmetrical fibers," Electron. Lett., vol.22, no.3, pp.127–129, 1986.

[16] M. Koshiba and K. Saitoh, "Structural dependence of effective area and mode field diameter for holey fibers," Opt. Express, vol.11, no.15, pp.1746–1756, 2003.

[17] G. Labroille, B. Denolle, P. Jian, P. Genevaux, N. Treps, and J.-F. Morizur, "Efficient and mode selective spatial mode multiplexer based on multi-plane light conversion," Opt. Express, vol.22, no.13, pp.15599–15607, 2014.

[18] M.B. Shemirani, W. Mao, R.A. Panicker, and J.M. Kahn, "Principal

modes in graded-index multimode fiber in presence of spatial- and polarization-mode coupling," J. Lightwave Technol., vol.27, no.10, pp.1248–1261, 2009.

Yuta Wakayama received M.E. and Ph.D. degrees in information science and technology from Hokkaido University, Sapporo, Japan, in 2010 and 2013, respectively. After graduation, he joined KDDI Corporation, Tokyo, Japan. Since 2014, he has been working at KDDI R&D Laboratories (currently KDDI Research), Inc., Saitama, Japan. His research interests include space-division multiplexed optical fiber transmission systems. Dr. Wakayama is a member of the Institute of Electronics, Information and Communication Engineers (IEICE) of Japan.

Hidenori Taga received B.E. and Ph.D. degrees in electronics engineering from the University of Tokyo, Tokyo, Japan in 1986 and 1998, respectively. In 1988, he joined Kokusai Denshin Denwa (KDD) R&D Laboratories, Tokyo, Japan, where he had engaged in research of undersea optical fiber communication systems employing optical amplifier repeaters. In 1998, he moved to KDD Submarine Cable Systems Inc., Tokyo, Japan, where he engaged in the development of undersea optical fiber communication systems using wavelength division multiplexing technology. In 2006, he moved to National Sun Yat-Sen University, Kaohsiung, Taiwan, where he engaged in research and education of optical fiber communication technology. In 2014, he joined KDDI R&D Laboratories (currently, KDDI Research), Inc., Saitama, Japan. Dr. Taga is a senior member of the Institute of Electronics, Information, and Communication Engineers in Japan.

Takehiro Tsuritani received M.E. and Ph.D. degrees in electronics engineering from Tohoku University, Miyagi, Japan, in 1997 and 2006, respectively. He joined Kokusai Denshin Denwa (KDD) Company, Limited (currently KDDI Corporation), Tokyo, Japan, in 1997. Since 1998, he has been working at their Research and Development Laboratories (currently KDDI Research, Inc.) and has been involved in research on high-capacity long-haul wavelength division multiplexing transmission systems and dynamic photonic networking. He is currently working as a senior manager of Photonic Transport Network Laboratory, KDDI Research, Inc. Dr. Tsuritani is a senior member of the Institute of Electronics, Information and Communication Engineers (IEICE) of Japan, and received the Best Paper Award of OECC 2000.